MICROSCOPY

Microscopy **62(4)**: 467–474 (2013)
doi: 10.1093/jmicro/dft020

Editor's Choice Article

Visualization of two distinct states of disassembly in the bacterial V–ATPase from *Thermus thermophilus*

Kazutoshi Tani[1], Christopher P. Arthur[2,3], Masatada Tamakoshi[4,5], Ken Yokoyama[6], Kaoru Mitsuoka[7], Yoshinori Fujiyoshi[1,8] and Christoph Gerle[9,*]

[1]Cellular and Structural Physiology Institute, Nagoya University, Nagoya 464-8601, Japan, [2]Department of Cell Biology, The Scripps Research Institute, 10550 North Torrey Pines Road, La Jolla, CA 92037, USA, [3]FEI Company, PO Box 80066, 5600 KA Eindhoven, The Netherlands, [4]Department of Molecular Biology, Tokyo University of Pharmacy and Life Sciences, 1432-1 Horinouchi, Hachioji, Tokyo 192-0392, Japan, [5]RIKEN SPring-8 Center, Harima Institute, 1-1-1 Kouto, Sayo, Hyogo 679-5148, Japan, [6]Department of Molecular Biosciences, Kyoto Sangyo University, Kamigamo-Motoyama, Kita-ku, Kyoto 603-8555, Japan, [7]Biomedical Information Research Center (BIRC), The National Institute of Advanced Industrial Science and Technology (AIST), 2-3-6 Aomi, Koto-ku, Tokyo 135-0064, Japan, [8]Department of Medicinal Science, Graduate School of Pharmaceutical Sciences, Nagoya University, Nagoya 464-8601, Japan and [9]Career Path Promotion Unit for Young Life Scientists, Kyoto University, Konoe-cho, Sakyo-ku, Kyoto 606-8501, Japan
*To whom correspondence should be addressed. E-mail: gerle.christoph@gmail.com

Abstract V-ATPases are multisubunit, membrane-bound, energy-converting, cellular machines whose assembly and disassembly is innately connected to their activity *in vivo*. *In vitro* V-ATPases show a propensity for disassembly that greatly complicates their functional, and, in particular, structural characterization. Direct structural evidence for early stages of their disassembly has not been reported yet. We analyzed the structure of the V-ATPase from *Thermus thermophilus* in a single negatively stained two-dimensional (2-D) crystal both by electron tomography and by electron crystallography. Our analysis demonstrated that for 2-D crystals of fragile macromolecular complexes, which are too heterogenous or too few for the merging of image data from many crystals, single-crystal 3-D reconstructions by electron tomography and electron crystallography are expedient tools of analysis. The asymmetric unit in the 2-D crystal lattice contains two different V-ATPase complexes that appear to be in an early stage of disassembly and with either one or both peripheral stalks not being visualized, suggesting the involvement of the peripheral stalks in early stages of disassembly.

Keywords rotary ATPase, 2D crystal, electron microscopy, tilt-series, labile protein complex, dissociation

Received 8 February 2013, accepted 14 March 2013; online 9 April 2013

Introduction

A multitude of cellular tasks are fulfilled by so-called cellular machines. Cellular machines are large macromolecular assemblies marked by the concerted interplay of multiple protein subunits, subcomplexes and co-factors, often involving relative intra-complex movements on the nanometer scale. Prominent examples are the ribosome, the spliceosome, fatty acid synthase, the proteasome, pyruvate dehydrogenase complex and rotary ATPases (F- and V-ATPases). Their readily changing assembly state in the living cell is often an important means of

regulating their activity. This, however, is often concomitant with a high degree of fragility, impacting on the experimenter's ease to extract an intact and homogenous sample from the cell for functional and structural characterization.

V-ATPases are a member of the family of membrane-bound energy converters termed rotary ATPases. These molecular machines are comprised of a cytosolic, water-soluble V_1 domain that acts as an ATP-driven rotary stepping motor coupled by peripheral and central stalks to a membrane-bound V_o domain that acts as an electric-energy-driven rotary stepping motor [1,2]. In eukaryotes, V-ATPases are dedicated proton pumps whose physiological role is to maintain the pH homeostasis of cellular compartments so as to enable various cellular functions such as receptor recycling, antigen processing, lysosomal protein degradation, synaptic vesicle neurotransmitter uptake or vacuolar transport [3,4]. In the non-respiring bacterium *Enterococcus hirae*, V-ATPase acts as a primary sodium pump, and recently the first high-resolution structures of its V_1 complex have been reported [5,6].

A unique mode of regulation in eukaryotic V-ATPase is the reversible dissociation of the V_1 and V_o domains [7]. It has been suggested that a prominent role in the reversible dissociation is played by its three peripheral stalks that connect the ATPase catalytic V_1 domain with its proton pumping, membrane-bound V_o domain [8–10]. Recent structural evidence suggests that among the three peripheral stalks of the enzyme in yeast, one might play a role as a primer for V-ATPase disassembly [11]. The V-ATPase from the eubacteria *Thermus thermophilus* (sometimes termed A-ATPase) presents a minimal version of the complex with a subunit stoichiometry of A_3B_3DF for the V_1 domain [12] and $IL_{12}CE_2G_2$ for the V_o domain [13,14]. Though its physiological role is the synthesis of ATP [15] and reversible dissociation is not part of its in vivo activity regulation, homology of its EG peripheral stalk subunits and the so-called non-homologous region of its catalytic A subunit allow comparison to eukaryotic V-ATPase.

The existing methods for structural investigation of biological macromolecular complexes necessitate the averaging of signal from many identical complexes. Early stages of disassembly in cellular machines are rarely characterized by stable intermediates and as a consequence are marked by heterogeneity between individual complexes. Hence, structural insights into early stages of disassembly processes, whether they are of physiological or non-physiological nature, remain scarce.

Electron crystallography and electron tomography are both techniques of molecular electron microscopy that are productive means of studying the structure of membrane protein complexes [16]. Previously, we succeeded in growing well-ordered two-dimensional (2-D) crystals of the V-ATPase from the eubacteria *T. thermophilus* through a 10-day, three-step crystallization procedure [17]. In the first step (I), dialysis at acidic pH resulted in multi-layered aggregates. (II) Large single layer sheets were formed after change to a cold, basic buffer. (III) Ordered arrays appeared after a brief heat-annealing step. A schematic representation and electron micrographs of the specimen at the three stages of the procedure are shown in Figure 1. However, heterogeneity of crystal packing and the low number of crystals found on electron microscopic grids limited our structural analysis of negatively stained crystals to a projection map calculated from merged non-tilted micrographs.

Here we report 3-D reconstructions of a single negatively stained 2-D crystal both by electron tomography and by electron crystallography, which clarify the crystal's packing and reveal two states of *T. thermophilus* V-ATPase disassembly.

Methods

2D crystallization and specimen preparation

Intact V-ATPase was purified from *T. thermophilus* and 2-D crystals grown as previously described [17] (Figure 1). Shortly after crystal formation, V-ATPase 2-D crystals were absorbed onto continuous carbon-film-coated copper grids, which were glow-discharged and stained with 2% uranyl acetate. Fifteen-nanometer gold fiducial markers were added to the back of the carbon film.

Electron microscopy

Images were recorded using a Tecnai F-30 microscope (FEI, Eindhoven, Netherlands) equipped with a post-column energy filter (GIF) and a $2K \times 2K$ CCD camera (Gatan, Pleasanton, CA). Tilt series were recorded using the automated acquisition

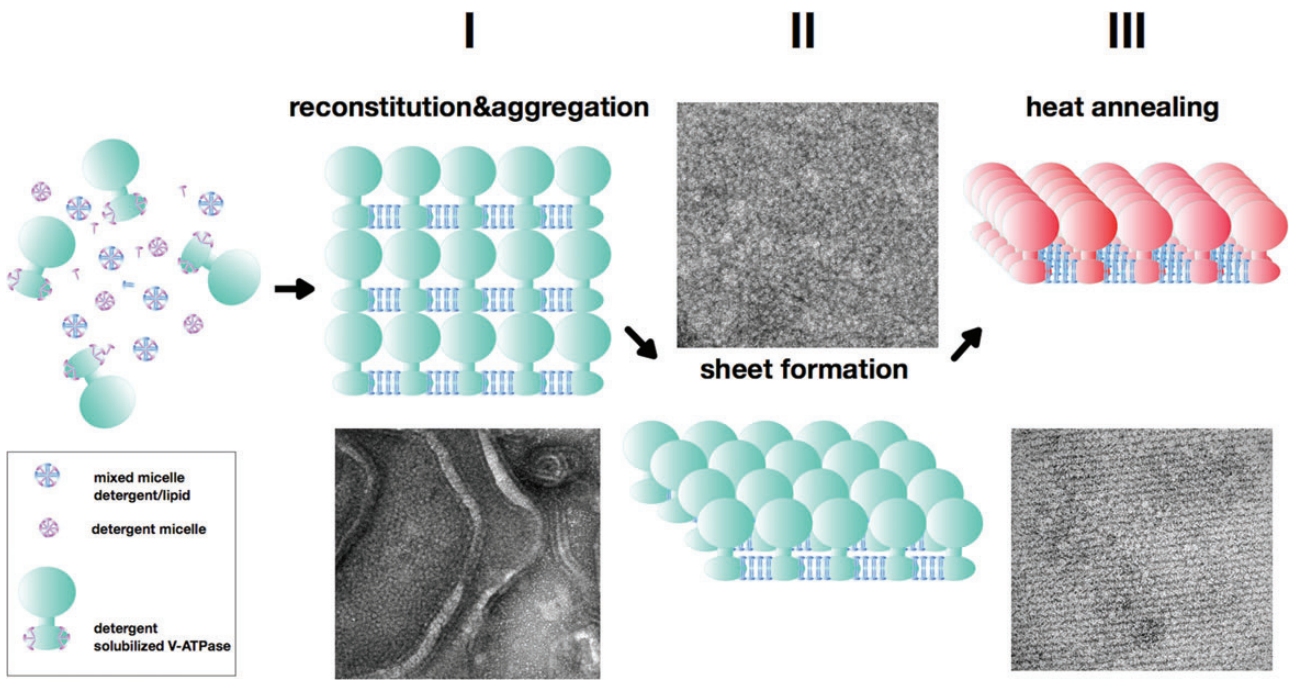

Fig. 1. To grow 2-D crystals of the *Thermus thermophilus* V-ATPase from mixed micelles of detergent-solubilized V-ATPase and lipids, a three-step dialysis protocol was employed. Dialysis at acidic pH resulted in multilayered aggregates (I), which formed large single-layer sheets after change to a cold, basic buffer (II), which exhibited ordered arrays (III) after a brief heat-annealing step. The resulting 2-D crystals were very fragile and disappeared in a few hours. A key motivation for this study was to gain structural insights at molecular level of why the obtained 2-D crystals were both defective and short-lived.

software SerialEM [18]. A series of 101 tilted images, starting at +55°, were collected at ×40,000 magnification, corresponding to a pixel size of 6.1 Å, every 1° until −55°, and then the sample was rotated 90° and the process was repeated.

Image processing for electron crystallographic reconstruction

The collected CCD images were transformed into MRC format. All the images were processed with the MRC 2D crystal processing package [19] to correct lattice distortions [20]. The contrast transfer function of each image was checked by whether its CTF zero was beyond a 15 Å resolution, using square frequency filtering in combination with periodogram averaging [21]. All the data were merged using LATLINE [22] at an 18 Å resolution. EM density maps of V_1V_o ATPase have been deposited in the EMDataBank (http://www.em.databank.org/: accession code EMD-2328).

Image processing for tomographic reconstruction

The eTomo graphical user interface of the IMOD tomography package [18,22] was used to calculate the 3-D reconstruction. The images in the tilt series were aligned using the gold fiducial markers and the final tomogram was calculated by weighted back projection.

All figures and movies were prepared using either UCSF Chimera [23] or the IMOD tomography package [22].

Results

A total of 212 images were taken of a single negatively stained *T. thermophilus* V-ATPase 2-D crystal on a double axis tilt series in one-degree steps ranging from −55° to +55° and −60° to +40°, respectively (see Supplementary movies S1 and S2). The tomographic reconstruction provides a 3-D overview of the crystal sheet in which a high degree of patchiness and crystal defects are easy to discern (Supplementary movie S3). Perhaps the most striking feature in the tomogram is the clearly visible A_3B_3 hexamers in some of the z-slices of the reconstruction (Figure 2).

A 3-D density map was successfully calculated from the area of highest order in the crystal sheet (outlined in Figure 2) by electron crystallographic reconstruction using all the images taken in the

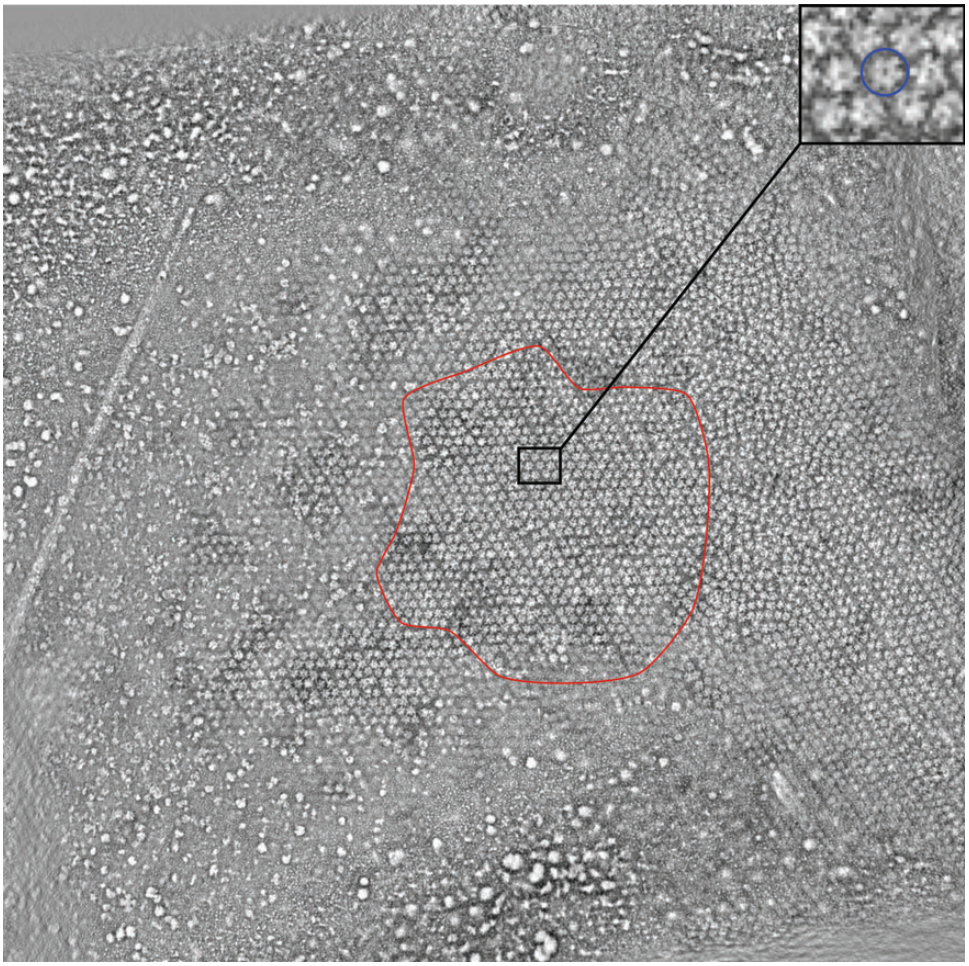

Fig. 2. Z-slice of the tomogram at a height at which the A_3B_3 hexamer of V-ATPase complexes in the crystal area that was used for the electron crystallographic reconstruction are clearly visible. The area of highest coherence is marked by a red line and a central area of the crystal is shown enlarged in the upper right inset with one A_3B_3 hexamer encircled in blue.

dual axis tilt series. Non-tilted micrographs for both axes, their Fourier transforms and representative lattice lines are shown in figure 3. The quality of the lattice lines and a low phase residual of 25° (14° for weighted IQ values) demonstrate the high quality of the reconstruction (Table 1). Figure 4 shows the two complexes of one unit cell depicted in blue and gold, which for the following will be termed blue and gold complexes, respectively. Interestingly, the two V-ATPase complexes of the unit cell are not identical and show distinctly different features. As a consequence, the crystallographic symmetry is reduced to p1 and earlier assumptions of the higher crystallographic symmetry of $p22_12_1$ based on a projection map have to be corrected. The V_1 domain is discernible by the strong density of the A_3B_3 hexamer in both complexes of the unit cell. A strong central density connects the V_1 domain to a lower oval-shaped density, which we identify as the central stalk and the V_o domain, respectively. In the blue complex, an additional density that connects the V_1 with the V_o domain peripherally is assumed to stem from one of the two peripheral EG stators. This peripheral stalk density is missing in the gold complex, which instead shows a bulging density in V_1 that does not connect to V_o. Another additional density is seen between the V_1 domains of the blue and the gold complexes, possibly stemming from a disconnected and disordered EG stator. Both complexes feature a strong tilt of the V_1 domain with respect to the V_o domain. In addition to this tilt, the central stalk of the blue complex appears to be twisted along its axis. Additionally, a side-view of the unit cell reveals that both complexes are tilted with respect to the x–y-plane of the crystal by 45° (Fig. 4c).

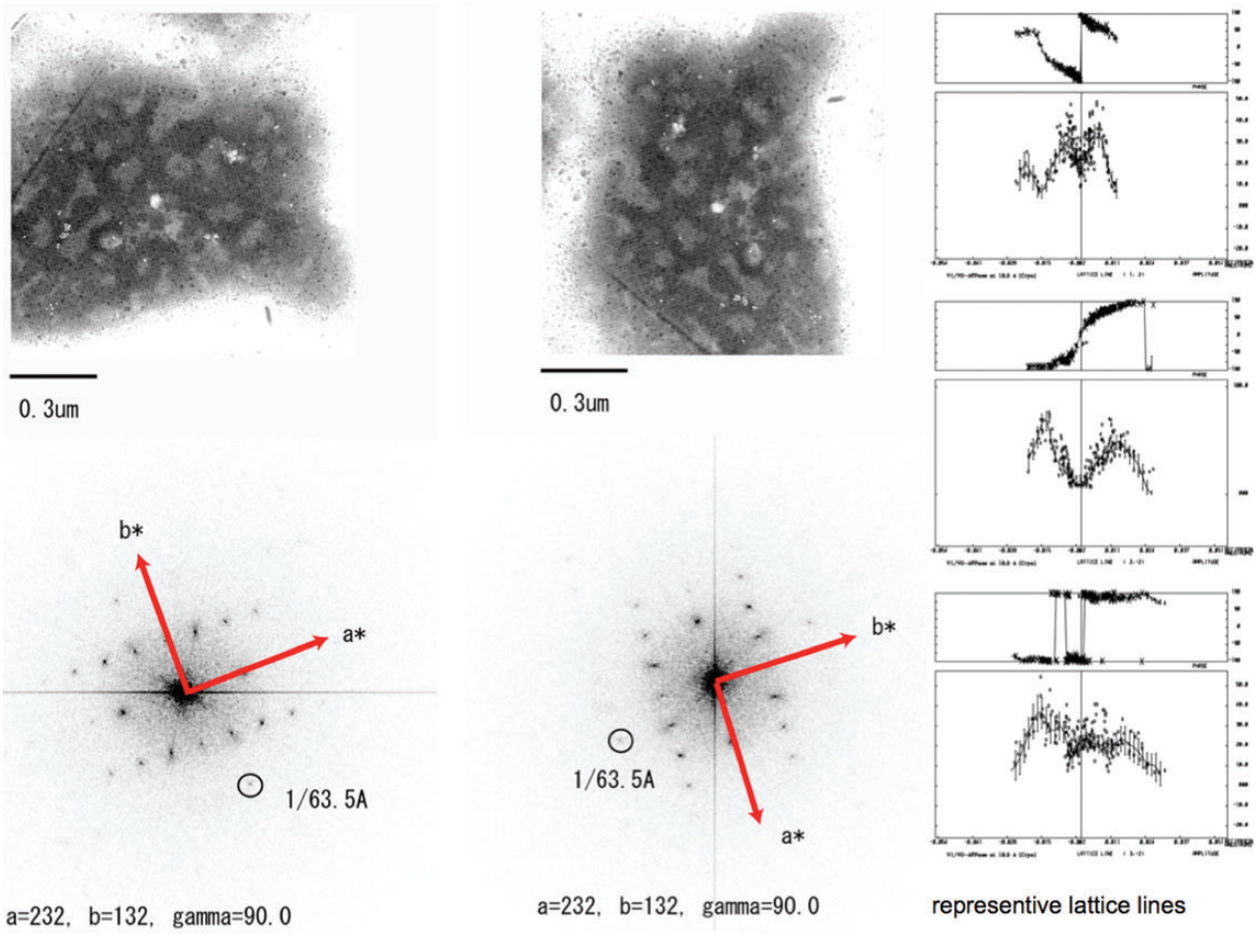

Fig. 3. Left panels: non-tilt images of the crystal sheet and their Fourier transform from both axis of the tilt-series with unit cell size and orientation in Fourier space indicated. Right panels: representative lattice lines of the crystallographic reconstruction.

Table 1. Electron crystallographic data

Space group	*p*1
Tilt angle range (increment angle)	−55° to +55° (+1°) −60° to +40° (+1°)
Number of images	212
Cell parameter (Å)	$a = 232$, $b = 132$, $\gamma = 90°$
Total number of observed reflections	14,270
Overall phase residuals (weighted IQ): IQ ≤ 6	25.2 (14.8)

Discussion

Our previous analysis of 2-D crystals grown from the *T. thermophilus* V-ATPase, though limited to non-tilt data, already revealed heterogeneity in unit cell size between individual crystals [17]. With the 3D reconstruction of a single 2-D crystal now at hand, it becomes clear that the observed heterogeneity between individual crystals likely originates from heterogeneity in the intactness of the individual V-ATPase complexes. The non-intactness of both complexes in the crystal's assymetric unit is apparent from the strong kink between the V_1 and V_o domains, exceeding 50° in the blue complex, and the absence of density for one or both peripheral stalks. These features are in stark contrast to the straight connection between the V_1 and the V_o domains and the presence of two peripheral stator stalks visualized in single-particle reconstructions of detergent-solubilized intact *T. thermophilus* V-ATPase [24–26] or even the wobbling movement that is thought to occur during rotary catalysis in the intact enzyme [27]. We speculate that the long dialysis time during the crystallization process and possibly also the changes in pH and temperature have caused the fragile V-ATPase complex to start to disassemble. Thus, the crystal offers a glimpse of an intermediate disassembly state that is characterized by a loosening of peripheral stalks, but, has

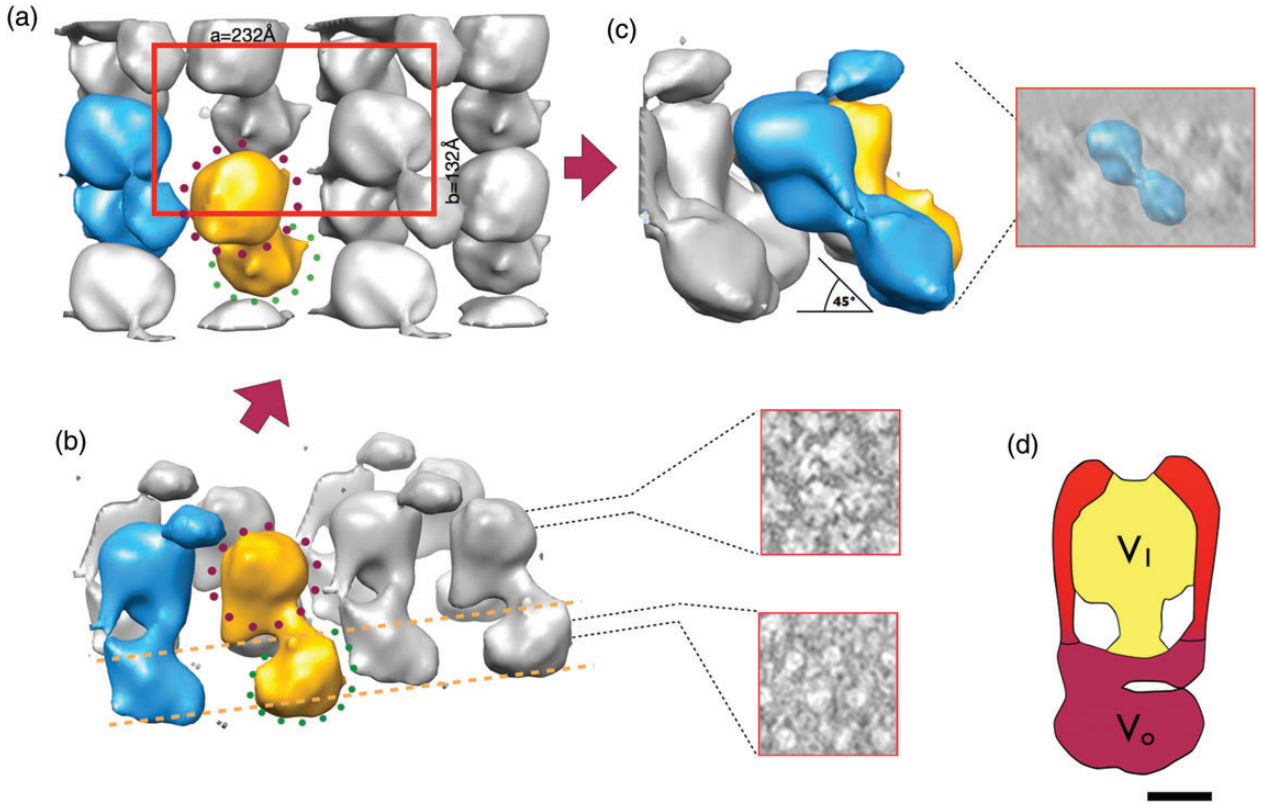

Fig. 4. The crystallographic reconstruction. (a) Projection view of the crystal with the unit cell outlined in red and the two V-ATPase complexes depicted in blue and gold. The V_1 domain and the V_o domain of the gold complex are indicated by purple and green dots, respectively. (b) Side view of the b-axis side of the same region turned ~30° anti-clockwise. The gold complex V_1 domain is connected to the V_o domain by only one strong central density, whereas the blue complex shows one additional peripheral connection. The rough position of the membrane is indicated by two yellow dashed lines. Z-slices in the tomogram at the height of the A3B3 hexamer or the V_o domain are indicated by dashed black lines and shown in two inset panels on the right. (c) Side view of the a-axis side. The strong 45° inclination of both V-ATPase complexes with respect to the *x*–*y*-crystal plane is clearly visible. The corresponding view in the tomogram with the blue complex inserted for comparison is shown in the inset panel on the right. (d) Schematic representation of the intact *T. thermophilus* V-ATPase drawn from EMD-1888 of the intact complex with the V_1 domain in yellow, the V_o domain in dark red and the peripheral stalks depicted in lighter hues. The scale bar represents 50 Å.

not yet advanced to the point of complete separation of the V_1 and the V_o domains. The two complexes in the unit cell do both maintain a central stalk connection between the V_1 and the V_o domains, but appear to have lost one or both peripheral stalk connections to the A_3B_3 complex. Absence of peripheral stalk density is not necessarily caused by physical absence, but rather indicates disorder through dislocation. The reported stability of the *T. thermophilus* V_o complex comprising subunits $IE_2G_2CL_{12}$ [13] makes a dislocation from the A_3B_3 complex interface the likeliest cause of missing peripheral stalk density. This prompts us to speculate that loosening of only one EG complex from the A_3B_3 complex is enough to destabilize the V_1-to-V_o connection and start complete disassemble via detachment of the second peripheral stalk, and finally the central stalk. This interpretation is in agreement with the experimentally observed short-lived nature of the 2-D crystals. Thus, we think that the observed disassembly states present a meta-stable state mainly stabilized by the heat-annealing-induced crystal contacts. We, therefore, propose that the in vitro disassembly of V_1 and V_o is not a random process, but rather goes through three distinct stages that involve, first, a stepwise release of EG complexes and then the dissociation of the central stalk DF subunit's foot from the rotor ring connected C subunit. This proposed sequence of events in the disassembly of the *T. thermophilus* V-ATPase complements a recent study that probed the association of V_1 and V_o by FRET analysis and highlighted the important role of the EG peripheral stalk for the intact complexes stability [28].

Experimental conditions in our study are far removed from the actual physiological conditions relevant during the in vivo disassembly of the *T. thermophilus* V-ATPase and even farer from the process of controlled, reversible dissociation in eukaryotic V-ATPases. Still, it is tempting to see the common importance of the peripheral stalks as not being a coincidence, but as an indication that one of the peripheral stalks serves as a preferred point of departure for the whole process of V-ATPase disassembly.

Variation in the disassembly states in the crystal sheet is likely also a prime cause of many patchy areas and a large number of point defects visible in z-slices of the tomographic reconstruction of the crystal sheet. The observed high tilt of 45° to the crystal's x–y-plane is the root cause of our previous deduction that the crystals unit cell contains four instead of two complexes and is of $p22_12_1$ instead of p1 symmetry. The high tilt of the V-ATPase complexes in the crystal is also difficult to accommodate with the previously assumed lipid bilayer reconstitution. Since the low critical micellar concentration detergent Triton X-100 was used as the solubilizing amphiphile during V-ATPase purification, a reasonable interpretation of the observed high tilt is that the complexes in the 2-D crystal are not embedded in a lipid bilayer but are rather surrounded by a bicelle of Triton X-100 and lipid. From the above-described experience, we have to conclude that correct interpretation of projection maps calculated from 2-D crystals grown from multisubunit membrane complexes, especially when they contain large extra-membranous domains, is not trivial and is prone to mistakes.

Considering the detailed insights we gleaned into the crystal packing and molecular content of the unit cell, we find that electron tomography and electron crystallographic reconstructions from a single negatively stained crystal can be powerful analytical tools in efforts that challenge the crystallization of large, fragile cellular machines.

Concluding remarks

In this study, we have shown that a combination of electron tomography and electron crystallography can be employed to yield detailed insights into the crystal packing of a single negatively stained 2-D crystal grown from macromolecular complexes. In addition, our electron crystallographic reconstruction offers a first glimpse of two early stages of in vitro disassembly of the eubacterial V-ATPase from *T. thermophilus*. The visualization of only two and one stalk connections suggests a sequential disassembly of the three stalks that connect the V_1 and the V_o domains in the intact complex.

Supplementary data

Supplementary data are available at http://jmicro.oxfordjournals.org/.

Acknowledgements

The authors thank Masasuke Yoshida for stimulating discussion and encouragement.

Funding

This work was supported by Grants-in-Aid for Young Scientists (B) (to K.T.); Grants-in-Aid for Scientific Research (S) (to Y.F.); the Japan New Energy and Industrial Technology Development Organization (NEDO) (to Y.F.) and the Special Coordination Fund for Promoting Science and Technology of MEXT, Japan (to C.G.) and a Platform for Drug Design, Discovery and Development grant from MEXT, Japan (to C.G.). Funding to pay the Open Access publication charges for this article was provided by the Platform for Drug Design, Discovery and Development grant from MEXT, Japan to Christoph Gerle.

References

1 Muench S P, Trinick J, and Harrison M A (2011) Structural divergence of the rotary ATPases. *Q. Rev. Biophys.* **44**: 311–356.

2 Junge W, Sielaff H, and Engelbrecht S (2009) Torque generation and elastic power transmission in the rotary F(O)F(1)-ATPase. *Nature* **459**: 364–370.

3 Toei M, Saum R, and Forgac M (2010) Regulation and isoform function of the V-ATPases. *Biochemistry* **49**: 4715–4723.

4 Jefferies K C, Cipriano D J, and Forgac M (2008) Function, structure and regulation of the vacuolar (H+)-ATPases. *Arch. Biochem. Biophys.* **476**: 33–42.

5 Murata T, Yamato I, and Kakinuma Y (2005) Structure and mechanism of vacuolar Na^+-translocating ATPase from *Enterococcus hirae*. *J. Bioenerg. Biomembr.* **37**: 411–413.

6 Arai S, Saijo S, Suzuki K, Mizutani K, Kakinuma Y, Ishizuka-Katsura Y, Ohsawa N, Terada T, Shirouzu M, Yokoyama S, Iwata S, Yamato I, and Murata T (2013) Rotation mechanism of *Enterococcus hirae* V (1)-ATPase based on asymmetric crystal structures. *Nature* **493**: 703–707.

7 Kane P M (2011) Targeting reversible disassembly as a mechanism of controlling V-ATPase activity. *Curr. Protein Pept. Sci.* **13**: 117–123.

8 Muench S P, Huss M, Song C F, Phillips C, Wieczorek H, Trinick J, and Harrison M A (2009) Cryo-electron microscopy of the vacuolar ATPase motor reveals its mechanical and regulatory complexity. *J. Mol. Biol.* **386**: 989–999.

9 Diepholz M, Venzke D, Prinz S, Batisse C, Flörchinger B, Rössle M, Svergun D I, Böttcher B, and Féthière J (2008) A different conformation for EGC stator subcomplex in solution and in the assembled yeast V-ATPase: possible implications for regulatory disassembly. *Structure* **16**: 1789–1798.

10 Diepholz M, Börsch M, and Böttcher B (2008) Structural organization of the V-ATPase and its implications for regulatory assembly and disassembly. *Biochem. Soc. Trans.* **36**: 1027–1031.

11 Oot R A, Huang L S, Berry E A, and Wilkens S (2012) Crystal structure of the yeast vacuolar ATPase heterotrimeric EGC(head) peripheral stalk complex. *Structure* **20**: 1881–1892.

12 Numoto N, Hasegawa Y, Takeda K, and Miki K (2009) Inter-subunit interaction and quaternary rearrangement defined by the central stalk of prokaryotic V(1)-ATPase. *EMBO Rep.* **10**: 1228–1234.

13 Yokoyama K, Nagata K, Imamura H, Ohkuma S, Yoshida M, and Tamakoshi M (2003) Subunit arrangement in V-ATPase from *Thermus thermophilus*. *J. Biol. Chem.* **278**: 42686–42691.

14 Toei M, Gerle C, Nakano M, Tani K, Gyobu N, Tamakoshi M, Sone N, Yoshida M, Fujiyoshi Y, Mitsuoka K, and Yokoyama K (2007) Dodecamer rotor ring defines H+/ATP ratio for ATP synthesis of prokaryotic V-ATPase from *Thermus thermophilus*. *Proc. Natl Acad. Sci. USA* **104**: 20256–20261.

15 Nakano M, Imamura H, Toei M, Tamakoshi M, Yoshida M, and Yokoyama K (2008) ATP hydrolysis and synthesis of a rotary motor V-ATPase from *Thermus thermophilus*. *J. Biol. Chem.* **283**: 20789–20796.

16 Stahlberg H and Walz T (2008) Molecular electron microscopy: state of the art and current challenges. *A.C.S. Chem. Biol.* **3**: 268–281.

17 Gerle C, Tani K, Yokoyama K, Tamakoshi M, Yoshida M, Fujiyoshi Y, and Mitsuoka K (2006) Two-dimensional crystallization and analysis of projection images of intact *Thermus thermophilus* V-ATPase. *J. Struct. Biol.* **153**: 200–206.

18 Mastronarde D N (2005) Automated electron microscope tomography using robust prediction of specimen movements. *J. Struct. Biol.* **152**: 36–51.

19 Crowther R A, Henderson R, and Smith J M (1996) MRC image processing programs. *J. Struct. Biol.* **116**: 9–16.

20 Henderson R, Baldwin J M, Downing K H, Lepault J, and Zemlin F (1986) Structure of purple membrane from *Halobacterium halobium*: recording, measurement and evaluation of electron micrographs at 3.5 Å resolution. *Ultramicroscopy* **65**: 31–44.

21 Agard D A A (1983) Least-squares method for determining structure factors in the three-dimensional tilted-view reconstructions. *J. Mol. Biol.* **167**: 849–852.

22 Kremer J R, Mastronarde D N, and McIntosh J R (1996) Computer visualization of three-dimensional image data using IMOD. *J. Struct. Biol.* **116**: 71–76.

23 Pettersen E F, Goddard T D, Huang C C, Couch G S, Greenblatt D M, Meng E C, and Ferrin T E (2004) UCSF Chimera—a visualization system for exploratory research and analysis. *J. Comput. Chem.* **25**: 1605–1612.

24 Bernal R A and Stock D (2004) Three-dimensional structure of the intact *Thermus thermophilus* H+-ATPase/synthase by electron microscopy. *Structure* **12**: 1789–1798.

25 Lau W and Rubinstein J (2010) Structure of intact *Thermus thermophilus* V-ATPase by cryo-EM reveals organization of the membrane-bound VO motor. *Proc. Natl Acad. Sci. USA.* **107**: 1367–1372.

26 Lau W and Rubinstein J (2011) Subnanometre-resolution structure of the intact *Thermus thermophilus* H(+)-driven ATP synthase. *Nature* **481**: 214–218.

27 Stewart A G, Lee L K, Donohoe M, Chaston J J, and Stock D (2012) The dynamic stator stalk of rotary ATPases. *Nat. Commun.* **3**: 687.

28 Kishikawa J and Yokoyama K (2012) Reconstitution of vacuolar-type rotary H+-ATPase/synthase from *Thermus thermophilus*. *J. Biol. Chem.* **287**: 24597–24603.